energies

MDPI

Article

Gas Hydrate and Free Gas Concentrations in Two Sites inside the Chilean Margin (Itata and Valdivia Offshores)

Vargas-Cordero Iván [1,*] iD **, Tinivella Umberta** [2] iD **and Villar-Muñoz Lucía** [3]

[1]   Facultad de Ingeniería, Universidad Andres Bello (UNAB), Quillota 980, 2531015 Viña del Mar, Chile
[2]   Istituto Nazionale di Oceanografia e di Geofisica Sperimentale (OGS), Borgo Grotta 42C, 34010 Trieste, Italy; utinivella@inogs.it
[3]   GEOMAR, Helmholtz Centre for Ocean Research, Wischhofstr 1-3, 24148 Kiel, Germany; lucia.villar@gmail.com
*   Correspondence: ivan.vargas@unab.cl; Tel.: +56-950-598-066

Abstract: Two sectors, Itata and Valdivia, which are located in the Chilean margin were analysed by using seismic data with the main purpose to characterize the gas hydrate concentration. Strong lateral velocity variations are recognised, showing a maximum value in Valdivia offshore (2380 ms^{-1} above the BSR) and a minimum value in the Itata offshore (1380 m·s^{-1} below the BSR). In both of the sectors, the maximum hydrate concentration reaches 17% of total volume, while the maximum free gas concentration is located Valdivia offshore (0.6% of total volume) in correspondence of an uplift sector. In the Itata offshore, the geothermal gradient that is estimated is variable and ranges from 32 °C·km^{-1} to 87 °C·km^{-1}, while in Valdivia offshore it is uniform and about 35 °C·km^{-1}. When considering both sites, the highest hydrate concentration is located in the accretionary prism (Valdivia offshore) and highest free gas concentration is distributed upwards, which may be considered as a natural pathway for lateral fluid migration. The results that are presented here contribute to the global knowledge of the relationship between hydrate/free gas presence and tectonic features, such as faults and folds, and furnishes a piece of the regional hydrate potentiality Chile offshore.

Keywords: gas hydrate; BSR; seismic velocity; gas-phase concentration; pre-stack depth migration; Chilean margin

1. Introduction

Many studies related to gas hydrate occurrences worldwide have been reported mainly to better characterize reservoirs, their potential as energy resource and the role gas hydrate can play in global climate change [1–3]. Concerning the former, large amounts of methane gas can be trapped in form of gas hydrate being considered as an important greenhouse gas. It is estimated that over a 20-year period, one ton of methane has a global warming potential 84–87 times greater than carbon dioxide and over a century, this warming potential is 28–36 times greater, according to the Intergovernmental Panel on Climate Change [4]. For these reasons, in the last decades, several projects have been carried out to assess the global methane hydrate quantities. The estimation of the global methane reservoir has decreased, while the knowledge about hydrate reservoirs have increased. Actually, few authors estimated 11,000 Gt of carbon in hydrate [5], while the last estimations are significantly lower [2,6–8].

The main indicator of gas hydrate occurrences in seismic sections is the bottom simulating reflector (BSR), which represents the boundary between the high seismic velocity gas hydrate-bearing sediments and the low seismic velocity underlying free gas [9,10].

Along the Chilean margin, the BSR has been identified along the accretionary prism [6–16]. During the Ocean Drilling Program (ODP) Leg 141, close to the Chile triple junction, it was discovered average

concentrations of 18% and 1% of volume of gas hydrate and free gas concentrations, respectively [17]. Nowadays, in the literature, a limited number of studies are performed to quantify gas hydrate in marine sediments along the Chilean margin [17–22]. However, a regional estimation is needed in order to map the gas-phase distribution along this margin.

It is well known that the presence of gas hydrate and/or free gas in the pore space of marine sediments can be detected analysing P-wave and S-wave velocity [23,24]. In fact, knowing the relationship between hydrate saturation in the pore space of sediments and elastic velocity, it is possible to convert seismic velocity section into gas-phase section. Several theoretical and empirical models are available in literature; here, we briefly overview the ones that are most commonly used. The empirical model of Ref. [25] is based on a weighted equation model. The first theory that includes the concept of cementation caused by the hydrate presence in proximity of the grains was proposed by [26]; as observed by Ref. [27] this theory predicts much higher seismic velocities than those that are normally observed in nature. The theory proposed by Ref. [28] considered the hydrate as a part of the skeleton; they verify the effective medium theory by using the ODP data (Leg 164, site 995, Blake Ridge area). The most used models were compared by Ref. [29]; they concluded that the main difference among resulting velocities versus gas hydrate concentration is not related to the empirical or theoretical approach adopted, but to the petrophysical properties hypothesized. In this study, the method proposed by [30,31] was adopted; it is based on the Biot-Gerstmann-Smith equation and was successfully verified by using direct measurements (i.e., Ocean Drilling Program—ODP, Leg 146 and 164; [23,32]) that gives results in agreement with the three-phase Biot theory [33].

The study area is located in Itata and Valdivia offshores along the Chilean continental slope between 36° S and 40° S (Figure 1), which is characterized by the subduction of the oceanic Nazca Plate below the South American continental plate along the Peru-Chile trench. The rate of subduction is estimated by Ref. [34–36], and is of about 66 km·Ma^{-1}.
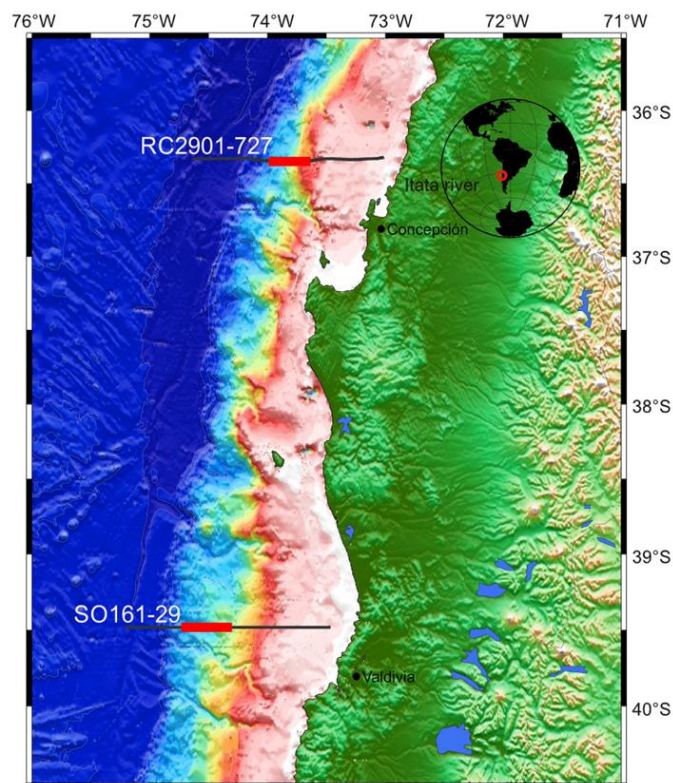

Figure 1. Location map of the two analysed seismic sections (black lines). The red segments indicate the analysed parts.

The objective of this study is improve the gas hydrate knowledge along the Chilean continental margin. For this, two seismic profiles were analysed. One line is located in the northern sector, Itata offshore, and a second one in the southern sector, Valdivia offshore (Figure 1). Our main goals are to estimate the gas hydrate and free gas concentrations on the studied area by using seismic information and theoretical models in order to obtain a regional map of the distribution of gas hydrates along the margin.

Our method includes: (1) calculation of the velocity field through iteratively pre-stack depth migration; (2) geological evaluation of velocity anomalies; and, (3) estimate gas hydrate and free gas concentrations by means of background velocity (i.e., velocity in failing of gas hydrates and free gas in the pore space) and theoretical model. Then, knowing seafloor and BSR depths, and seafloor temperature, the geothermal gradient was calculated.

2. Material and Methods

2.1. Seismic Data

The seismic profiles used in this study were acquired by the Research Vessel (RV) Sonne (January–February 2001) during the project SPOC (Subduction Processes off Chile) and by the RV Conrad (January–February 1988) during the ODP project "Mid-Ocean Spreading Ridge (Chile Ridge)". Two seismic lines were analysed here: RC2901-727 and SO161-29 (Figure 1).

Seismic processing was performed by using Seismic Unix (SU, [37]) software (43R8, The Center for Wave Phenomena (CWP), Golden, CO, USA). The profile RC2901-727 was collected with a 3000-m long streamer, formed by 240 channels every 12.5 m. The seismic origin was an adjusted assemble of ten airguns with a total volume of 61.3 L, and a shot spacing of 50 m. The SO161-29 seismic line was acquired using a 3000-m long streamer with 132 channels; the inter-trace was variable: the first 24 channels are characterized by an inter-trace of 12.5 m, while the remaining channels were separated by 25 m. The adopted seismic source was a tuned array that was constituted by 20 airguns with a total volume of 54.1 L; the shot spacing was 50 m.

2.2. Advanced Processing and Inversion Modelling

After the identification of the BSR in the post-stacked sections, a part of each seismic line (about 20 km) was selected to perform advanced processing in the area where the BSR signature was the strongest and most continuous. The base of the free gas layer reflector, the so called BGR [18], that can be identify below the BSR, was also locally detected. We adopted a procedure that has already tested in several geological contexts in order to determine the gas hydrate and free gas presences and their amount [17,19,23,38,39].

The main goal was to get an accurate velocity model by using the layer stripping approach [35,40]. In this methodology, the layers are modelled in depth by using iteratively a Kirchhoff pre-stack depth migration (PreSDM) (see details in Ref. [16]).

The initial velocity model is assumed as constant and equal to the water velocity estimated by seismic data (1480 m s^{-1}). We defined the horizontal and vertical spacing of the grid equal to 10 and 12.5 m, respectively, for the RC2901-727 section, and 10 and 25 m for the SO161-29 section. To determine the seismic velocity model, several horizons in depth are selected when considering continuous reflectors. The method used to determine the velocity model consists to perform PreSDM. The reliability of the final velocity field is verified analysing the flatness of the horizons in the Common Image Gather (CIG) domain. In the case of not-flatness of the reflections in the CIG domain, the velocity model was updated by using the [41] approach and a new PreSDM was performed. PreSDM, analysis of the CIGs and velocity update are performed iteratively until the final velocity model is reliable. The reliability of the final velocity model is confirmed by the small difference between the depths at near and far offset of all reflections [17]. A velocity gradient was included below the last inverted reflector, i.e., the free gas reflector (BGR), and the so-obtained velocity models were smoothed before

performing the final PreSDM. The migration is more stable if the velocity model is smoothed [41]. The gas hydrate and free gas quantities were estimated using models before smoothing. The large offsets were characterized by stretching effects, and with the main purpose being to improve the final seismic imaging, we produced stacked sections of the CIGs when considering only the offset of less than 2500 m. The final stacked sections of the CIGs were obtained after the application of a trace mixing and a band-pass filter. Details about the number of iterations necessary to estimate the velocity for each layer is reported in Table 1.

Table 1. Details about the number of iterations necessary to obtain the final velocity model for each layer of the two analysed seismic lines.

Seismic Line	Modelledm Layers (Top-Bottom)	Number of Iterations
RC2901-727	Seawater-seafloor	4
	Seafloor-BSR	30
	BSR-BGR	10
SO161-29	Seawater-Seafloor	6
	Seafloor-Horizon 1	25
	Horizon 1-BSR	45
	BSR-BGR	BGR not recognisable

2.3. BSR-Derived Geothermal Gradient

The geothermal gradient (defined as dT/dZ) can be evaluated by using the following formula:

$$dT/dZ = (T_{BSR} - T_{SEA})/(Z_{BSR} - Z_{SEA}),$$

where T_{BSR} and T_{SEA} are the temperatures at the BSR and the seafloor, respectively, Z_{BSR} and Z_{SEA} are the BSR and the seafloor depths, respectively [42]. The BSR and the seafloor depths were obtained by seismic data analysis; the seafloor temperature (equal to 2.2 °C) was extracted from instruments used to measure the conductivity, temperature, and pressure of seawater (CTD) off Chile [42]; the seawater salinity was assumed equal to 35%. To determine the temperature at the BSR, we considered the gas hydrates dissociation temperature-pressure function proposed by [43,44]; knowing the pressure (i.e., depth) at the BSR the temperature is determined by the hydrate dissociation function. We assumed that gas hydrate is formed by methane; note that this is to assume the most restrictive case (i.e., shallower BSR). Moreover, as suggested by other studies [16], the effect of the very small presence of ethane (about 1%; [45]) can be neglected.

2.4. Estimate of Gas Hydrate and Free Gas Concentrations

The gas-phase amounts can be estimated by converting the velocity anomalies (i.e., the difference between the estimated seismic velocity and the theoretical background velocity curve evaluated for water saturated sediments) in terms of gas hydrate and free gas concentrations. In the case of anomalous high velocity, we assumed the presence of gas hydrates, whereas if anomalous low velocity was detected, the free gas presence was modelled. As mentioned before, the theoretical velocity was calculated adopting the method described in Refs. [30,31]. In our case, the main error is due to the sediment property assumptions due to the lack of direct measurements and not to the adopted theoretical approach. By fitting the theoretical velocity to the experimental velocity (velocity model obtained by PreSDM), and increasing the parameters of the theoretical model that are related to the gas-phase concentrations, we obtained a quantitative estimation. The adopted approach can model two main free gas distributions in the pore space: uniform distribution (i.e., gas and water in pore space) and patchy distribution (i.e., all gas in patches without water). Because of the detected anomalous low velocity, our estimates are modelled while considering a uniform distribution [31]. The background

velocity was modelled by using porosity and density information reported by Ref. [46] assuming an initial porosity of 60% measured from ODP drilling [42,47].

3. Results

3.1. Velocity Model and PreSDM Sections

By comparing the background velocity with the velocity models, it is possible to recognise above the BSR a high velocity layer (1900–2380 m·s^{-1}) that is associated to gas hydrate presence.

In the northern sector, below where the BSR low velocity layer was recognised (1380–1450 m·s^{-1}), which can be associated with the free gas presence (Figure 2, upper panel). Both of the sections are characterised by strong lateral velocity variations. In Itata offshore, the lowest velocity below the BSR is reached in correspondence to the uplift sector (see Figure 2 in the upper panel from 8 to 13 km), while a high velocity above the BSR is present Valdivia offshore in two sectors (see Figure 2 in the lower panel from 2 to 5 km and from 12 to 15 km). Note the low velocity that is just below the seafloor detected in the southern sector in correspondence of faults and fractures (Figure 2, lower panel).
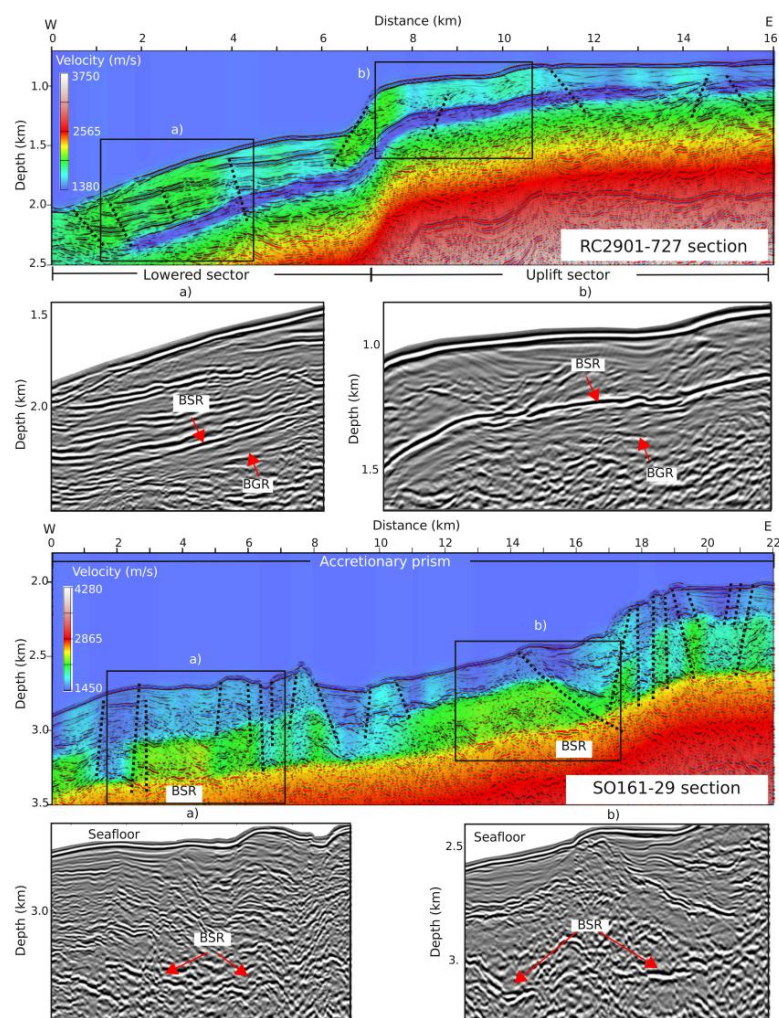

Figure 2. Velocity model superimposed to the Kirchhoff pre-stack depth migration (PreSDM) sections of the northern (**upper** panel) and southern (**lower** panel) sectors. The rectangles in the sections indicate the position of the zooms (a and b), in which the bottom simulating reflector (BSR) and the free gas reflector (BGR) (if present) are indicated by red arrows. Faults and fractures are indicated by dotted lines.

The BSR is strong and continuous along the Itata section, while it is weak and discontinuous along the Valdivia section. It misses where there are evidences of features of intense deformations, such as by faults and fractures that cut sediments reaching the seafloor (see Figure 2; lower panel, SO161-29 section). Moreover, a variable BSR depth was recognised across RC2901-727 section (Figure 2, upper panel), reaching maximum value in the downwards part (400 m below seafloor; mbsf) and the minimum value upwards part (200 mbsf), whereas a constant BSR depth was recognised across SO161-29 section close to 550 mbsf. The PreSDM section of the northern sector (RC2901-727 section) allowed for the estimation of gas hydrate and free gas thicknesses of about 220 m and 80 m, respectively. On the contrary, in the southern sector (SO161-29 section) only gas hydrate thickness can be estimated (270 m) because of BGR is not recognisable (Figure 2, lower panel).

Finally, as mentioned before, the BGR is present along most parts of the northern seismic section and it indicates the base of the free gas layer, which is characterised by low velocity. As underlined in the blow-up in Figure 2 (upper panel, RC2901-727 section), the observed loss of reflectivity below the BGR could due to the absorption caused by the free gas presence.

3.2. BSR-Derived Geothermal Gradient

As discussed in the previous section, the geothermal gradient was estimated by using BSR depths, and the results were variable in the northern sector (RC2901-727 section), with a maximum value equal to 87 °C km^{-1} in the uplift sector, and a minimum value equal to 32 °C km^{-1} in the western sector (Figure 3, upper panel). So, this section presents two geothermal regimes: relative low/high geothermal gradient in the western/eastern part respectively. On the contrary, in the southern sector, a quite constant geothermal gradient is present along the whole analysed section, with value of about 35 °C km^{-1} (lower panel in Figure 3; SO161-29 section).
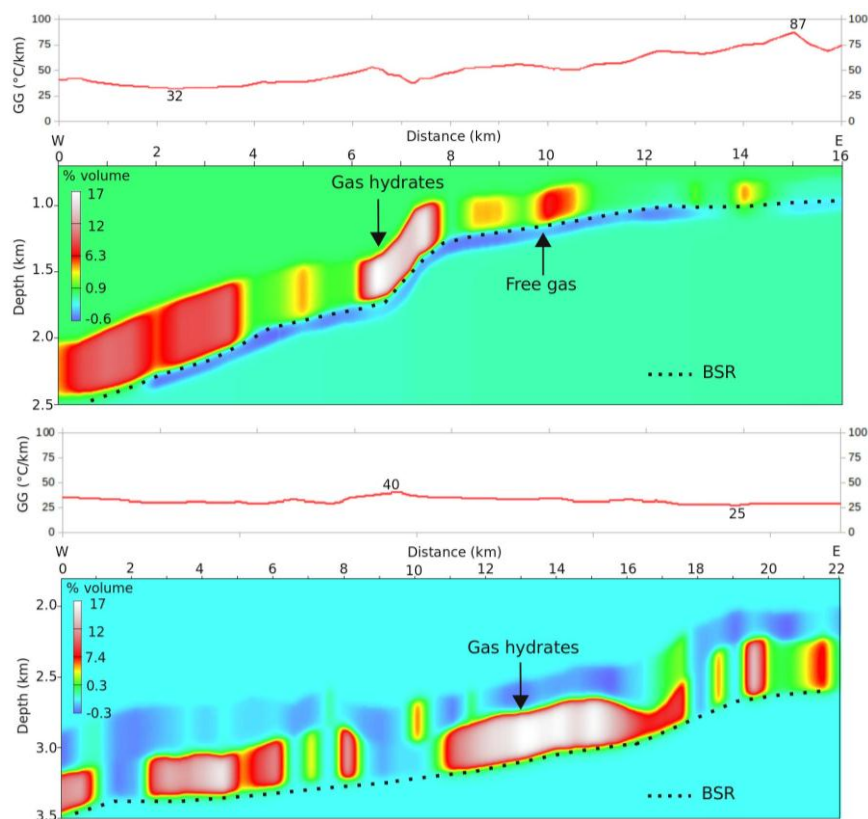

Figure 3. Gas hydrate (positive values) and free gas (negative values) concentration models. The BSR is indicated by dotted lines. GG (red lines) indicates the geothermal gradient estimated by BSR depth. See text for details. The numbers reported across the red line indicate the upper and lower GG values.

3.3. Estimate of Gas Hydrate and Free Gas Concentration

Results of the gas-phase estimate indicate a high variability along the sections, particularly in the northern sector (Figure 3). The highest gas hydrate concentration is about 17% of total volume in both northern and southern sectors. In the northern sector (RC2901-727 section), the gas hydrate concentration is negligible in the uplift sector (from 8 to 14 km; Figure 3 upper panel), while it varies from 5% to 17% in the western part. The free gas distribution is opposite to that of gas hydrates in this section. The highest concentration (0.6% of total volume) is located close to the uplift sector, while the concentration decreases (0.1% of total volume) in the areas where the gas hydrate amount increases (from 6 to 8 km; see Figure 3 upper panel). In the southern sector (SO161-29 section), the highest gas hydrate concentrations ranging 10% to 17% of total volume are recognised from 3 to 5 km and from 12 to 15 km (Figure 3 lower panel). In general, in this sector the hydrate amount variability is less pronounced. Note that small amounts of free gas are estimated just below the seafloor because of low velocity presence. Unlike other analysed section, it was not possible to characterize the free gas distribution because of the BGR is not recognisable.

4. Discussion

From the analysis of the seismic sections, two tectonic domains can be recognised. The first one in the northern sector is associated with low tectonic activity and is characterized by few faults and fractures (Figure 2, upper panel). The second one is located in the southern sector that is related to high tectonic activity, showing many faults and fractures (Figure 2, lower panel). As evidenced in the southern sector (SO161-29 section), small slips across faults and fractures affecting the shallowest sediments suggest that these structures are actives. In the northern sector (RC2901-727 section), one main fault of about 7 km configures an uplift sector vs. a western sector. As a consequence, this uplift can explain lateral and depth variation of the BSR that is presented in this sector, which is caused by the temperature variation of the sediments due to the intense fluids up-welling. A variable BSR depth (400 to 200 mbsf; Figure 2 upper panel) can be explained supposing a variable geothermal gradient (from 32° to 87 °C km; Figure 3 upper panel). On the other hand, in the southern sector (SO161-29 section), the BSR is deeper (550 mbsf). Here, the higher BSR depth (compared to the northern sector) can be explained by highest water depth (i.e., pressure) and lower geothermal gradient (about 35 °C km). It is important to notice that the geothermal gradient values that are reported in the literature [11,12,17,19,20] are in agreement with our results.

The seismic velocity analysis in both sections indicates strong lateral variations, which is consistent with previous observations (i.e., [17–19]). In fact, above the BSR the lowest velocity is observed in correspondence to faults and fractures (SO161-29 section), which may be justified with a porosity variation along accretionary prism [16]. In the northern sector (RC2901-727 section), the seismic character suggests finer grained lithology in correspondence of uplift sector, whereas in the western sector, the stratified sediments may be associated with slide or turbidite deposits (Figure 2, upper panel). This assumption is in correspondence with lithological researches that were performed in the southernmost part by Ref. [48]. Besides, the highest velocity that was calculated in both seismic profiles can be explained by two main factors: (1) the gas hydrate existence; and (2) the change in petro-physical properties as a result of the differential compaction of marine sediments, which can be explained assuming high dewatering is caused due to faults and fractures presence or associated to the uplift [49]. In addition, as reported in literature (i.e., [50,51]), the porosity reduction and the consequent velocity increases can be caused by continental glaciations effects.

The northern sector (line RC2901-727) shows an opposite trend regarding the distribution of free gas. The highest free gas concentration (0.6% of total volume) is located in correspondence of the lowest gas hydrate concentration. In addition, the lowest velocity that was observed along uplift sector can be related to the accumulation of fluid in the pore space that migrated upwards from the western sector and/or possible hydrate dissociation (Figure 3, upper panel). This result is in agreement with the highest geothermal gradient that was estimated from seismic data (Figure 3, upper panel).

On the other hand, in the southern sector, the BGR absence can be explained by the presence of faults and fractures, which prevent fluids accumulation and cause fluid escapes. These phenomena are in agreement with the low velocity layer that was detected just below the seafloor and was converted in terms of free gas concentration (Figure 3, lower panel). In fact, this anomalous low velocity can be caused by two main factors: (1) the high fluid flux caused by the presence of faults and fractures that favour the fluid escape, and (2) the change of petro-physical properties (mainly an increase of porosity) that decrease the background velocity [17].

Gas-phase estimates derived from velocity models allow for concluding that the velocity above the BSR is caused by high gas hydrate concentrations, while the low velocity below the BSR observed in correspondence of uplift sector is caused by the high free gas concentration, as expected.

5. Conclusions

The gas hydrate and free gas estimate values that are reported in this paper are in agreement with the values reported by other authors [11,12,45], confirming that our procedure can be considered a useful tool to determine and characterize the gas-phase variability at regional scale. Moreover, our results confirm the inverse relationship between gas hydrate concentration and faults and fractures presence that have already been reported by several authors [52].

The high local concentrations of both hydrate (17%) and free gas (0.6%) detected in this, and previous studies could be considered to assess the energy resource potentiality Chile offshore. It is worth recalling that gas hydrate research development can play an important role along the Chilean margin due to the high seismicity that characterises this region. It is important to jointly map the hydrate occurrence and the seismicity in order to correctly evaluate the geohazard. In fact, as underlined by several authors [53], an earthquake can contribute to gas hydrate dissociation processes and trigger a marine slide.

In conclusion, our study gives a contribution regarding the global knowledge of the relationship between hydrate/free gas presence and tectonic features, such as faults and folds, and furnishes a piece of the regional hydrate potentiality Chile offshore.

Author Contributions: All authors were involved in the data processing and preparation process. All authors were involved in the discussion and revision process with section leads as follows: Iván Vargas-Cordero (Sections 1–5), Umberta Tinivella (Sections 3–5) and Lucia Villar-Muñoz (Sections 4 and 5)).

References

1. Kennett, J.P.; Cannariato, K.G.; Hendy, I.L.; Behl, R.J. Methane Hydrates in Quaternary Climate Change: The Clathrate Gun Hypothesis. In *Methane Hydrates in Quaternary Climate Change: The Clathrate Gun Hypothesis*; American Geophysical Union: Washington, DC, USA, 2003; pp. 1–217.

2. Milkov, A.V. Global estimates of hydrate—Bound gas in marine sediments: How much is really out there? *Earth Sci. Rev.* **2004**, *66*, 183–197. [CrossRef]

3. Moridis, G.J.; Collett, T.S.; Boswell, R.; Hancock, S.; Rutqvist, J.; Santamarina, C.; Kneafsey, T.; Reagan, M.; Pooladi-Darvish, T.M.; Kowalsky, M. Gas Hydrates as a Potential Energy Source: State of Knowledge and Challenges. *Adv. Biofuels Bioprod.* **2013**, 977–1033. [CrossRef]

4. IPCC. Contribution of Working Groups I, II and III to the Fifth Assessment Report of the Intergovernmental Panel on Climate Change. In *Climate Change 2014: Synthesis Report*; Pachauri, R.K., Meyer, L.A., Eds.; IPCC: Geneva, Switzerland, 2014; pp. 1–151. ISBN 978-92-9169-143-2.

5. Kvenvolden, K.A. Natural gas hydrate: Background and history of discovery. In *Natural Gas Hydrate in Oceanic and Permafrost Environments*; Max, M.D., Ed.; Kluwer Academic Publishers: Dordrecht, The Netherlands, 2000; pp. 9–16. ISBN 978-94-011-4387-5.

6. Burwicz, L.E.; Rüpke, B.H.; Wallmann, K. Estimation of the global amount of submarine gas hydrates formed via microbial methane formation based on numerical reaction-transport modeling and a novel parameterization of Holocene sedimentation. *Geochim. Cosmochim. Acta* **2011**, *75*, 4562–4576. [CrossRef]

7. Wallmann, K.; Pinero, E.; Burwicz, E.; Haeckel, M.; Hensen, C.; Dale, A.; Ruepke, L. The Global Inventory of Methane Hydrate in Marine Sediments: A Theoretical Approach. *Energies* **2013**, *5*, 2449–2498. [CrossRef]

8. Marin-Moreno, H.; Giustiniani, M.; Tinivella, U.; Pinero, E. The challenges of quantifying the carbon stored in Arctic marine gas hydrate. *Mar. Pet. Geol.* **2016**, *71*, 76–82. [CrossRef]

9. Hyndman, R.D.; Spence, G.D. A seismic study of methane hydrate marine bottom-simulating-reflectors. *J. Geophys. Res.* **1992**, *97*, 6683–6698. [CrossRef]

10. Mienert, J.; Bünz, S. Bottom Simulating Seismic Reflectors (BSR). Encyclopedia of Marine. *Geosciences* **2017**, 62–67. [CrossRef]

11. Bangs, N.L.; Brown, K.M. Regional heat flow in the vicinity of the Chile Triple Junction constrained by the depth of the bottom simulating reflector. In Proceedings of the Ocean Drilling Program, Scientific Results; Lewis, S.D., Behrmann, J.H., Musgrave, R.J., Cande, S.C., Eds.; Ocean Drilling Program: College Station, TX, USA, 1995; Volume 141, pp. 253–258. [CrossRef]

12. Brown, K.M.; Bangs, N.L.; Froelich, P.N.; Kvenvolden, K.A. The nature, distribution, and origin of gas hydrate in the Chile Triple Junction region. *Earth Planet. Sci. Lett.* **1996**, *139*, 471–483. [CrossRef]

13. Diaz–Naveas, J. Sediment Subduction and Accretion at the CHILEAN Convergent Margin between 35° and 40°S. Ph.D. Dissertation, University of Kiel, Kiel, Germany, 1999; pp. 1–130.

14. Grevemeyer, I.; Diaz–Naveaz, J.L.; Ranero, C.R.; Villenger, H.W. Ocean Drilling Program Scientific Party. Heat Flow over the descending Nazca plate in Central Chile, 32° S to 41° S: Observations from ODP Leg 202 and the occurrence of natural gas hydrates. *Earth Planet. Sci. Lett.* **2003**, *213*, 285–298. [CrossRef]

15. Morales, E. Methane hydrates in the Chilean continental margin. *Electron. J. Biotechnol.* **2003**, *6*, 80–84. [CrossRef]

16. Vargas–Cordero, I.C. Gas Hydrate Occurrence and Morpho—Structures along Chilean Margin. Ph.D. Dissertation, University of Trieste, Trieste, Italy, 2009; pp. 1–138.

17. Vargas-Cordero, I.; Tinivella, U.; Accaino, F.; Loreto, M.F.; Fanucci, F. Thermal state and concentration of gas hydrate and free gas of Coyhaique Chilean Margin (44°30′S). *Mar. Pet. Geol.* **2010**, *27*, 1148–1156. [CrossRef]

18. Vargas-Cordero, I.; Tinivella, U.; Accaino, F.; Fanucci, F.; Loreto, M.F.; Lascano, M.E.; Reichert, C. Basal and Frontal Accretion Processes versus BSR Characteristics along the Chilean Margin. *J. Geophys. Res.* **2011**, *2011*, 846101. [CrossRef]

19. Vargas Cordero, I.; Tinivella, U.; Villar Muñoz, L.; Giustiniani, M. Gas hydrate and free gas estimation from seismic analysis offshore Chiloé island (Chile). *Andean Geol.* **2016**, *43*, 263–274. [CrossRef]

20. Villar-Muñoz, L.; Behrmann, J.H.; Diaz-Naveas, J.; Klaeschen, D.; Karstens, J. Heat flow in the southern Chile forearc controlled by large-scale tectonic processes. *Geo-Mar. Lett.* **2014**, *34*, 185–198. [CrossRef]

21. Bangs, N.L.; Sawyer, D.S.; Golovchenko, X. Free gas at the base of the gas hydrate zone in the vicinity of the Chile triple Junction. *Geology* **1993**, *21*, 905–908. [CrossRef]

22. Rodrigo, C.; Gonzalez–Fernández, A.; Vera, E. Variability of the bottom-simulating reflector (BSR) and its association with tectonic structures in the Chilean margin between Arauco Gulf (37°S) and Valdivia (40°S). *Mar. Geophys. Res.* **2009**, *30*, 1–19. [CrossRef]

23. Tinivella, U.; Carcione, J.M. Estimation of gas hydrate concentration and free gas saturation from log and seismic data. *Lead. Edge* **2001**, *20*, 200–203. [CrossRef]

24. Bünz, S.; Mienert, J. Acoustic imaging of gas hydrate and free gas at the Storegga Slide. *J. Geophys. Res.* **2004**, *109*, 1–15. [CrossRef]

25. Lee, M.W.; Hutchinson, D.R.; Collett, T.S.; Dillon, W.P. Seismic velocities for hydrate-bearing sediments using weighted equation. *J. Geophys. Res. Solid Earth* **1996**, *101*, 20347–20358. [CrossRef]

26. Dvorkin, J.; Nur, A. Elasticity of high-porosity sandstones: Theory for two North Sea data sets. *Geophysics* **1996**, *61*, 1363–1370. [CrossRef]

27. Ecker, C.; Dvorkin, J.; Nur, A. Sediments with gas hydrates: Internal structure from seismic AVO. *Geophysics* **1998**, *63*, 1659–1669. [CrossRef]

28. Helgerud, M.B.; Dvorkin, J.; Nur, A.; Sakai, A.; Collett, T.S. Elastic wave velocity in marine sediments with gas hydrates: Effective medium modelling. *Geophys. Res. Lett.* **1999**, *26*, 2021–2024. [CrossRef]

29. Chand, S.; Minshull, T.A.; Gei, D.; Carcione, J.M. Elastic velocity models for gas hydrate bearing sediments a comparison. *Geophys. J. Int.* **2004**, *159*, 573–590. [CrossRef]

30. Tinivella, U. A method for estimating gas hydrate and free gas concentrations in marine sediments. *Boll. Geofis. Teor. Appl.* **1999**, *40*, 19–30.

31. Tinivella, U. The seismic response to overpressure versus gas 638 hydrate and free gas concentration. *J. Seism. Explor.* **2002**, *11*, 283–305.

32. Tinivella, U.; Lodolo, E. The Blake Ridge bottom simulating reflector transect: Tomographic velocity field and theoretical models to estimate hydrate quantities. In Proceedings of the Ocean Drilling Program, Scientific Results; Paull, C.K., Matsumoto, R., Wallace, P.J., Dillon, W.P., Eds.; Ocean Drilling Program: College Station, TX, USA, 2000; Volume 164, pp. 273–281. [CrossRef]

33. Carcione, J.M.; Tinivella, U. Bottom simulating reflectors: Seismic velocities and AVO effects. *Geophysics* **2000**, *65*, 54–67. [CrossRef]

34. Carcione, J.M.; Tinivella, U. The seismic response to overpressure: A modelling study based on laboratory, well and seismic data. *Geophys. Prospect.* **2001**, *49*, 523–539. [CrossRef]

35. Angermann, D.; Klotz, J.; Reiberg, C. Space—Geodetic estimation of the Nazca—South American Euler vector. *Earth Planet. Sci. Lett.* **1999**, *171*, 329–334. [CrossRef]

36. Kendrick, E.; Bevis, M.; Smalley, R., Jr.; Brooks, B.; Vargas, R.C.; Lauría, E.; Fortes, L.P.S. The Nazca–South America Euler vector and its rate of change. *J. South Am. Earth Sci.* **2003**, *16*, 125–131. [CrossRef]

37. Cohen, J.K.; Stockwell, J.W. *CWP/SU: Seismic Unix Release 4.0: A free Package for Seismic Research and Processing*; Center for Wave Phenomena, Colorado School of Mines: Golden, CO, USA, 2008; pp. 1–153.

38. Tinivella, U.; Loreto, M.F.; Accaino, F. Regional versus detailed velocity analysis to quantify hydrate and free gas in marine sediments: The south Shetland margin target study. *Geol. Soc. Spec. Publ.* **2009**, *319*, 103–119. [CrossRef]

39. Loreto, M.F.; Tinivella, U.; Accaino, F.; Giustiniani, M. Gas hydrate reservoir characterization by geophysical data analysis (offshore Antarctic Peninsula). *Energies.* **2011**, *4*, 39–56. [CrossRef]

40. Yilmaz, O. *Seismic Data Analysis: Processing, Inversion and Interpretation of Seismic Data*, 2nd ed.; Society of Exploration Geophysicists: Tulsa, OK, USA, 2001; pp. 1–2027. ISBN 978-1-56080-094-1.

41. Liu, Z.; Bleistein, N. Migration velocity analysis: Theory and an iterative algorithm. *Geophysics* **1995**, *60*, 142–153. [CrossRef]

42. Grevemeyer, I.; Villinger, H. Gas hydrate stability and the assessment of heat flow through continental margins. *Geophys. J. Int.* **2001**, *145*, 647–660. [CrossRef]

43. Dickens, G.R.; Quinby-Hunt, M.S. Methane hydrate stability in seawater. *Geophys. Res. Lett.* **1994**, *21*, 2115–2118. [CrossRef]

44. Sloan, E.D. *Clathrate Hydrates of Natural Gases*, 2nd ed.; Marcel Dekker, Inc.: New York, NY, USA, 1998; pp. 1–641, ISBN 0824799372.

45. Froelich, P.N.; Kvenvolden, K.A.; Torres, M.E.; Waseda, A.; Didyk, BM.; Lorenson, T.D. Geochemical evidence for gas hydrate in sediment near the Chile triple junction. In *Proceedings of the Ocean Drilling Program, Scientific Results*; Lewis, S.D., Behrmann, J.H., Musgrave, R.J., Cande, S.C., Eds.; Ocean Drilling Program: College Station, TX, USA, 1995; Volume 141, pp. 276–286. [CrossRef]

46. Hamilton, E.L. Sound velocity gradients in marine sediments. *J. Acoust. Soc. Am.* **1979**, *65*, 909–922. [CrossRef]

47. Mix, A.C.; Tiedemann, R.; Blum, P.; Abrantes, F.F.; Benway, H.; Cacho-Lascorz, I.; Chen, M.; Delaney, M.L.; Flores, J.A.; Giosan, L.; Holbourn, A.E.; et al. *Proceeding ODP Initial Reptorts 202*; Ocean Drilling Program: College Station, TX, USA, 2003. [CrossRef]

48. Marsaglia, K.M.; Torrez, X.V.; Padilla, I.; Rimkus, K.C. Provenance of Pleistocene and Pliocene sand and sandstone, ODP leg 141, Chile margin. In *Proceedings of the Ocean Drilling Program, Scientific Results*; Lewis, S.D., Behrmann, J.H., Musgrave, R.J., Cande, S.C., Eds.; Ocean Drilling Program: College Station, TX, USA, 1995; Volume 141, pp. 133–151. [CrossRef]

49. Loreto, F.M.; Tinivella, U.; Ranero, C.R. Evidence for fluid circulation, overpressure and tectonic style along the Southern Chilean margin. *Tectonophysics* **2007**, *429*, 183–200. [CrossRef]

50. Rabassa, J.; Clapperton, C. Quaternary glaciations of the Southern Andes, Quaternary glaciations in the Southern Hemisphere. *Quat. Sci. Rev.* **1990**, *9*, 153–174. [CrossRef]

51. Accaino, F.; Bohm, G.; Brancolini, G. Analysis of Antarctic glaciations by seismic reflection and refraction tomography. *Mar. Geol.* **2005**, *216*, 145–154. [CrossRef]

52. Loreto, M.F.; Tinivella, U. Gas hydrate versus geological features: The South Shetland case study. *Mar. Pet. Geol.* **2012**, *36*, 164–171. [CrossRef]

53. Boobalan, A.J.; Ramanujam, N. Triggering mechanism of gas hydrate dissociation and subsequent sub marine landslide and ocean wide Tsunami after Great Sumatra—Andaman 2004 earthquake. *Arch. Appl. Sci. Res.* **2013**, *5*, 105–110.